BULLETIN OF THE POLISH ACADEMY OF SCIENCES
TECHNICAL SCIENCES
DOI: 10.24425/bpasts.2024.151384

Assessing the equivalent spring modelling method of CFS elements encased in ultra-lightweight concrete

Ahmed Alabedi [1] Péter Hegyi [2]

[1] Ph.D. candidate, Department of Structural Engineering, Budapest University of Technology and Economics, Hungary, alabedi.ahmed@edu.bme.hu

[2] Assistant professor, Department of Structural Engineering, Budapest University of Technology and Economics, Hungary, *hegyi.peter@emk.bme.hu*

Abstract. An efficient finite element approach was recently developed to analyse encased cold-formed steel (CFS) structures. This new technique replaced encasing material with unidirectional springs, analogous to the Winkler foundation concept, to shorten the analysis time while ensuring accuracy and reliability in predicting the structural behaviour of encased CFS components. In this paper, the validity, and limitations of the simplified spring model to represent outstanding plates were assessed. The investigation demonstrated that the simplified spring model could effectively predict the ultimate load for a wide range of ultra-lightweight concrete moduli (50-250 MPa) with an acceptable error. The analysis indicated that plate elements initially in cross-section class 4 without encasing material become at least class 3, or better as a consequence of encasing. Previously reported experiments were used to evaluate the performance of the ESM. The analysis demonstrated that the ESM can accurately predict the local failure ultimate load of encased CFS sections with an acceptable error percent and significantly less computational effort than a 3D solid model.

Key words: plate buckling; numerical analysis; equivalent spring model; sustainability

1. INTRODUCTION AND AIMS

Nowadays, cold-formed steel (CFS) has become a preferable construction material for low- and mid-rise structures, serving as a more efficient alternative to traditional materials like hot-rolled steel and reinforced concrete. These cost-effective building systems, distinguished by significant benefits such as light weight, fast fabrication, easy manufacturing, and absence of formwork, contributed to the widespread use of CFS elements in various applications. Consequently, CFS elements have become extensively used as primary load-bearing structures in pallet racks, industrial facilities, and residential buildings [1], [2].

Serving as load-bearing elements, CFS components exhibit distinct failure mechanisms regarding stability (i.e., local, distortional, global buckling and interaction). Thus, extensive research efforts have been dedicated to enhance CFS performance, including intensive experimental and analytical works. Accordingly, incorporating concrete for filling and bracing stands out as a viable approach to enhance the performance and behavior of CFS elements. An even better configuration can be reached when the applied infill material has good heat insulation capacity, as this results in a sustainable structural system with double benefit: infill material (i) enhances the structural performance and (ii) improves the heating energy efficiency, too.

*e-mail: alabedi.ahmed@edu.bme.hu

For instance, in [3], [4], the impact of continuous bracing on the performance of composite CFS walls was deeply investigated under axial compressive loads utilizing lightweight flue gas desulfurization gypsum and phosphogypsum as infill material. Their experimental findings demonstrated that including lightweight fillers significantly enhances the axial compressive strength of CFS walls. Xu et al. [5], [6], [7] examined the high-strength lightweight foamed concrete (HLFC) impacts on the performance of CFS shear walls. Their findings highlighted a notable enhancement in seismic performance for infilled CFS composites, with a shift in failure mode from brittle to ductile in tested specimens. Similarly, Wang and colleagues [8], [9], [10] carried out experimental investigations on composite CFS shear walls using various filler materials, including lightweight polymer material (LPM) [8], [9] and light EPS mortars (LEM) [10]. Their results highlighted the significant impact of infill materials on the seismic behaviour, load-bearing capacity, and energy dissipation of shear walls.

In [11], [12], a different enhancement technique was implemented for corrugated steel sheets by continuous bracing using various formulations of foamed concrete. The findings demonstrated the substantial influence of the infill material, as the lightweight foamed concrete enhanced the structural response, leading to the development of a novel structural system with sufficient load-carrying capacity suitable for low-rise residential buildings. Similarly, Eltayeb et al. thoroughly

investigated the performance of profile double-skin steel composite walls (PSCW) when filled with foam and rubberized foam concrete (FRC) under axial [13] and eccentric compressive loads [14] while varying the rubber contents. Their research aimed to examine the structural behaviour of FRC-filled PSCWs comprehensively, and their study showed that FRC can effectively be used as a filling material, offering adequate capacities for residential building systems.

The performance of composite CFS under axial compression was further examined in [15] and [16] using engineered cementitious composites [15] and fibre-reinforced concrete [16]. The research results demonstrated the importance of composite columns, and the assessed specimens demonstrated noteworthy enhancements in compressive strength, ductility, and energy absorption. Furthermore, numerous studies have been undertaken in this field, with researchers combining CFS columns with different infill materials while considering varying section sizes, concrete strengths, and the impact of longitudinal stiffeners [17], [18], [19].

Recently, a novel cold-formed steel system was investigated at Budapest University of Technology, focused on improving the stability of CFS members. This innovative approach uses polystyrene aggregate concrete (PAC) as an encasing material [20]. Extensive tests were conducted on CFS flexural, compression elements and shear panels. The experiments revealed that PAC significantly impacts CFS's stability, improving its load-bearing capacity[2], [21], [22], [23].

The complexity of these components made their finite element (FE) representation more problematic and time-consuming. Thus, an efficient modelling technique is required which is able to reduce the computational cost of analysis. In response, Eid et al. developed a simplified finite element modelling technique for analysing encased CFS elements by replacing PAC with elastic unidirectional equivalent springs analogous to the Winkler foundation [24]. The technique is called the equivalent spring model, ESM. The equivalent spring stiffness was determined by comparing the FE critical buckling stress result to that calculated from the approximated equation in [1], [25]. The new modelling technique yielded satisfactory outcomes, but the performance in ultimate limit state was never investigated.

Our final aim is to make the ESM a universal tool for calculating the resistance of elastic material encased CFS elements of different cross section. As a first step , in [26], the validity and limitations of the ESM for internal plates having four simply supported edges were deeply investigated comparing the spring model results to a 3-D solid model.

The current research work continues the previously mentioned efforts and presents an extended study specifically for outstanding elements (plates with three simply supported and one free edge), aiming to acquire a deeper understanding of the ESM. The performance of this modelling technique will be compared against 3-D solid FE model (SMOD) for the case of elastic plate buckling and for ultimate load bearing capacity using GMNIA analysis. As a synthesis of results contained by this paper and [26] the ability of ESM to predict full cross-section resistance of compression elements will be discussed, too, using experimental data reported in [21], [22].

2. DEVELOPMENT OF NUMERICAL MODEL

For the PAC-encased C-section under axial compression (Figure 1 A), the web and flange of the C-section are internal components (Fig. 1 (B)). The numerical modelling of those

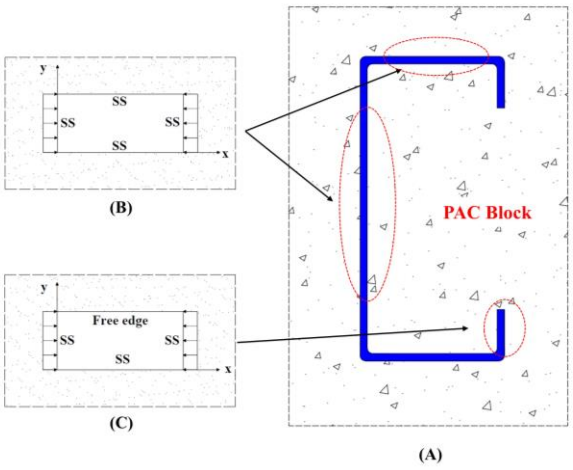

Fig. 1 (A) Braced CFS section (B) internal plate (C) outstand plate

elements was previously discussed in [26]. The stiffeners shown in Figure 1 (C) are considered outstanding elements and are represented in Eurocode effective width calculations as plates with three simply supported edges and one free edge. In this paper, two distinct encased outstanding plate FE models will be developed using ANSYS software [27], based on the modelling criteria outlined in EC3-1-5 [28].

The more complex model utilizes solid elements (SMOD) to simulate the elastic medium, while the simplified one replaces it with a calibrated equivalent spring (ESM). The SMOD will be used as reference model to the model of our interest, the ESM. There is an important mechanical difference between the two models. The SMOD utilizes 3-D solids, accounting for realistic stress distribution in the elastic medium based on the displacement of the plate. On the other hand, the ESM relies on a Winkler-type foundation; only normal stress is considered and it is solely associated with the displacement of the plate at a specific point [26]. To examine the validity and limitations of the ESM method, the parameters detailed in Table 1 were used in this study. The ultra-lightweight concrete modulus range is based on the material experiments reported in [21]. Mesh size is the steel plate and infill mesh size in the case of SMOD and the unsupported area between adjacent springs in ESM.

TABLE 1. Range of parameters of the numerical investigation

Parameter	Range
Steel plate slenderness (b/t)	20-60 extended to 10-60 in Chapter 4.2.
Yield strength of steel (f_y)	180-380 [MPa]
Infill elastic modulus (E_C)	50-250 [MPa]
Mesh size (A)	(5*5)-(20*20) [mm^2]

2.1. SMOD FEM development

The SMOD FEM plate geometry was simulated using 4-node shell elements (SHELL181), the material model was characterized by a bilinear stress-strain curve incorporating the von Mises yield criterion and isotropic hardening effects. The geometric configuration was set according to Table 1. To achieve long plate behaviour, the plate length (l_x) was assigned to be six times the estimated buckling length, as recommended in [1], [25]. Regarding boundary conditions, three of the plate edges were restrained in the out-of-plane direction (Z), with a single central node fixed in the cross direction (Y) to eliminate rigid body motion.

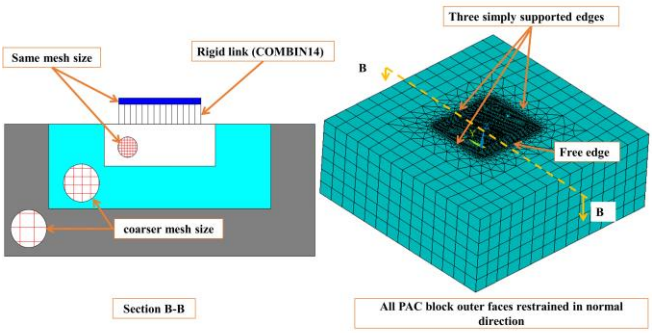

Fig. 2 SMOD FEM geometry

The elastic material (PAC in the experiments) was represented using the 8-node solid element SOLID185. Mesh size of the interior part was increased by 15 times towards the outside region to reduce computational demands (see Figure 2). Z directional 1D connection links (COMBIN14) perpendicular to the plate were generated between the plate and the solid underneath it, activated only by the relative motion of the plate and the solid in the Z direction (i.e. no friction or bonding is considered). The separation between the plate and the concrete was disregarded, as the infill material encases steel on both sides in reality. The outer faces of the infill block were restricted solely in the normal direction of the face. Material behavior was assumed to be linear elastic without considerations for cracking or crushing, according to previous findings in [1], [21], these phenomena primarily impact the post-failure behaviour of plates and not the failure itself.

The nonlinear analysis incorporated material nonlinearity and geometrical imperfections of the plate (GMNIA). Imperfections were defined as the first eigen-shape of the encased model and scaled by an amplitude of b/50, adhering to Eurocode recommendations.

2.2. ESM FEM development

The FE model described in section 2.1 was used to develop the simplified model (ESM) with the solid medium replaced by unidirectional springs. The COMBIN40 element was utilized to represent the foundation acting only in the Z-direction, as illustrated in Figure 3. Material nonlinearity and geometrical imperfections were considered when conducting the nonlinear analysis. Eq. (1) reported in [24] was used to calculate the required spring stiffness with E_C as Young's modulus of the elastic medium, A as steel mesh size area (it is also the unsupported area between adjacent springs), and lower-case a, b, c, d, e, and f constants as per Table 2. Note that the listed constants of Table 2 were derived based on curve fitting the results of linear buckling analysis to the predictions of Eq. (2) for various b/t ratios by Eid et al. [24]. Mind that for different b/t ratios, different coefficients have to be used. Eq. (2) is an approximated formula for calculating the critical buckling stress of encased plate in [1], [25], Where $\sigma_{cr,p}$ is the critical buckling stress of encased outstanding plate, b/t is plate slenderness ratio, E_s and v_s are steel plate elastic modulus, and Poisson's ratio.

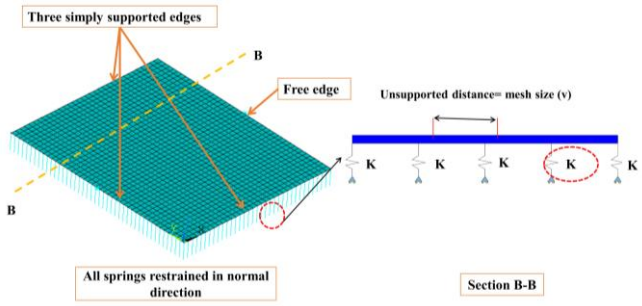

Fig. 3 ESM FEM geometry

$$K = a\left[\frac{N}{mm}\right] + b\left[\frac{N}{mm^3}\right]A + c[mm]E_c + d\left[\frac{N}{mm^5}\right]A^2 + e\left[\frac{1}{mm}\right]AE_c + f[\frac{mm^3}{N}]E_c^2 \quad (1)$$

$$\sigma_{cr,p} = 0.43\frac{\pi^2 E_S}{12(1-v_S^2)(b/t)^2} + \frac{1200MPa}{b/t} + 2.22E_c + \sqrt{E_c.3390} - 40 \quad (2)$$

3. VALIDATION OF THE NUMERICAL MODELS

The first step of the model validation process was of the unbraced plates. The assessment involved the critical stress (refer to Figure 4 A) and the normalized ultimate strengths of the plate (represented by $\chi = N_{u,FEM}/btf_y$, as shown in Figure 4 B) to Eurocode values. The critical stress values showed a precise fit (maximum error 4 %), the maximum relative deviation of the ultimate strength was 6.2%, which was found to be aligned well with previously documented findings in the literature database [29], [30], [31], [32], [33].

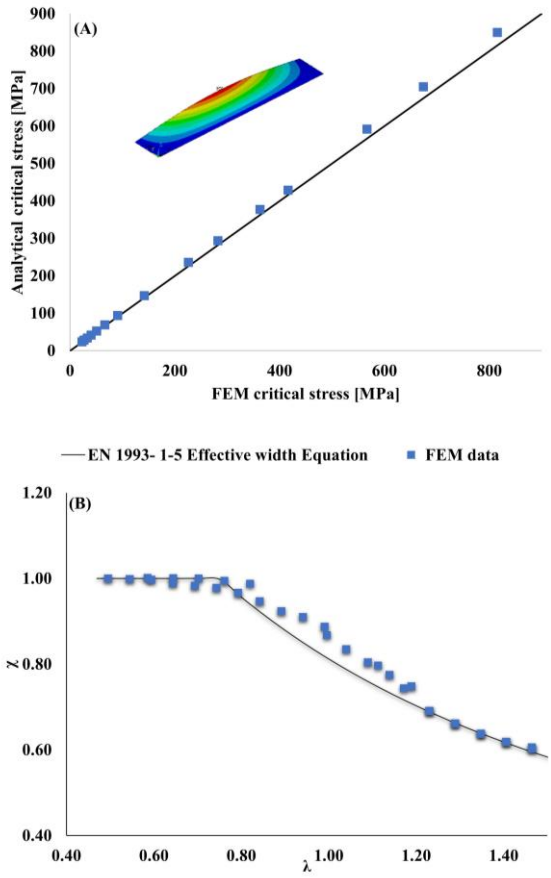

Fig. 4. Verification of FE model for outstanding plate A) At critical stress B) normalized ultimate strength

As a next step, ESM performance was evaluated, comparing the critical stresses obtained from the linear buckling analysis to analytical values of Eq. (2), an approximate equation reported in [1], [25]. The error of the approximate equation is less than 5 % on the full range, thus it is considered acceptable for the basis of validation.

It was observed that the error of the estimation of the ESM for critical stress is significantly influenced by the plate slenderness. The error of the ESM, as depicted in Fig. 5, varied from 8-16% for smaller b/t values, gradually decreasing to 5-10% for larger ratios, considering different elastic moduli E_C. The error is comparatively lower for larger b/t values, with lower E_C yielding a lower error. Nevertheless, the trend of the results illustrated in Fig. 5 revealed that the computed K values of Eq. (1) tend to overestimate the foundation stiffness.

TABLE 2 Coefficients of equation (2) of outstand plates [24]

b/t	a [N/mm]	b [N/mm^3]	c [mm]	d [N/mm^5]	e [1/mm]	f [mm^3/N]
20	-190.1	5.984	1.726	-0.03303	0.02399	0.001433
35	-231.1	3.485	2.906	-0.00814	0.01683	0.0004
50	-255.9	3.879	2.891	-0.0096	0.01908	0.000625
60	-269.9	3.735	3.024	-0.00816	0.02133	0.00022

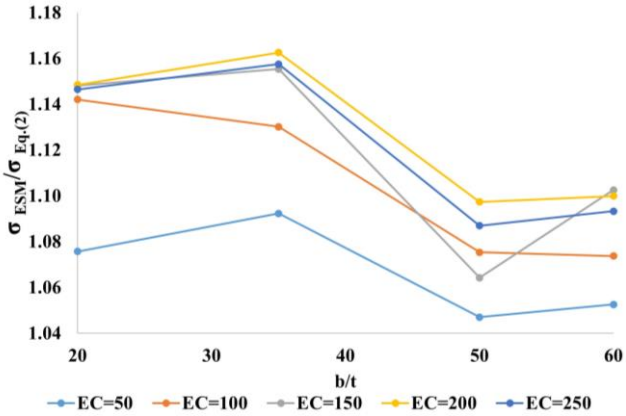

Fig. 5. Verification of ESM, error - b/t relation considering different elastic moduli

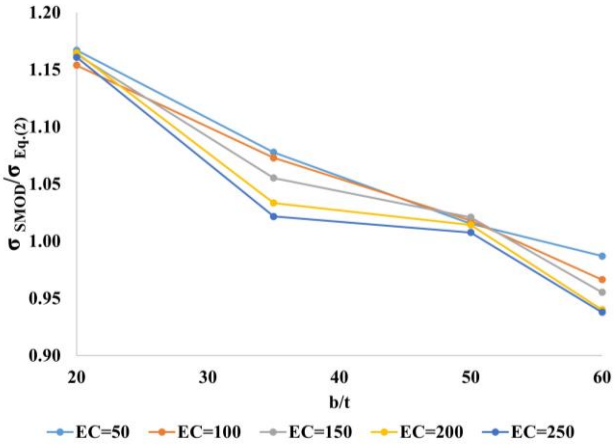

Fig. 6. Verification of SMOD, error - b/t relation considering different elastic moduli

Lastly, the SMOD linear buckling analysis results were compared to those derived from Eq. (2). The discrepancy in SMOD results ranged from 4 to 15% relative to Eq. (2), depending on plate slenderness and foundation stiffness. In Fig. 6, the SMOD results, and Eq. (2) calculated critical stress were compared. It can be noticed that better agreement was indicated for higher b/t values (e.g., b/t = 50 and beyond). In other words, the error gradually decreased as the b/t ratio increased, with a deviation of 4% observed at a b/t ratio of 60. However, the observed 15% error in critical stress results in a maximum 4.5% overestimation of the ultimate load-bearing capacity when using the Winter-curve of the Eurocode standard. Hence, the

observed difference is deemed acceptable; consequently, SMOD was utilized to assess the ultimate strength of braced plate elements. It is crucial to state that the verification process and initial results in section 4.1 will be constrained by Table 2; in section 4.2, the ESM application will be further extended, including a smaller b/t ratio.

4. EVALUATION OF ESM FOR ULTIMATE STRENGTH

4.1. Original procedure

The SMOD results are used as reference for the ESM model. The ultimate strength was identified by GMNIA. The analysis revealed that the ESM could match the SMOD results with a maximum discrepancy of 5 % in the investigated range. To exemplify the performance of the ESM, Figure 7 A illustrates the error as a function of b/t and E_C, respectively. Accordingly, the ESM is considered applicable in the investigated parameter range.

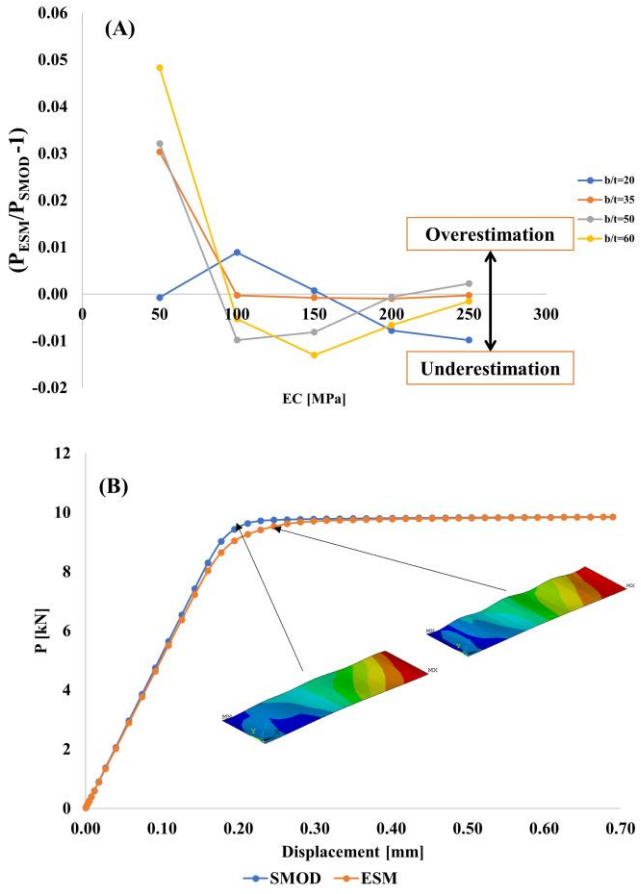

Fig. 7. A) ESM error, B) Load-displacement curve b/t = 35, E_C = 150

Furthermore, load-displacement curves and failure mechanisms were also compared. Fig. 7 B illustrates the load-displacement curves for b/t=35 and E_C=150 MPa plates; it can be noticed that both models predict that the plate element is not producing local buckling in the elastic domain. Therefore, it means that the plate element is no more in cross-section class 4. This behaviour can also be seen on Figure 8, where grey line represents the unstiffened plate, having elastic plate buckling.

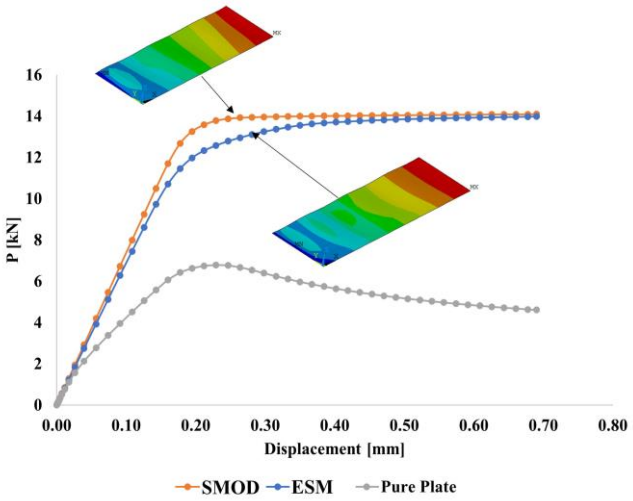

Fig. 8. Load-displacement curve b/t = 50, E_C = 150

4.2. Recalibration of spring stiffness

It is obvious that the ESM results are consistent with the SMOD results. Nevertheless, having multiple equations for limited b/t can be impractical and time-consuming. Similar to the authors work reported in [26], a parametric study has been conducted to identify a single formula that is able to represent the elastic foundation in the investigated b/t range. For outstanding plate, the analysis demonstrated that using constants corresponding to b/t = 50 value (Eq. (3)) is able to give acceptable results with maximum error of 6 % (see Figure 9). The initial lower limit for b/t of the method was 20. As real plate slenderness of outstand stiffeners can have smaller values than this, the proposed Eq. (3) was verified for b/t = 10 as well with good results.

Thus, the proposed equation can effectively calculate foundation stiffness in the range of PAC modulus (50–250 MPa) and (10-60) plate slenderness.

$$K = -255.9 + 3.897A + 2.981E_c - 0.0096A^2 + 0.01908AE_c + 0.000625E_c^2 \quad (3)$$

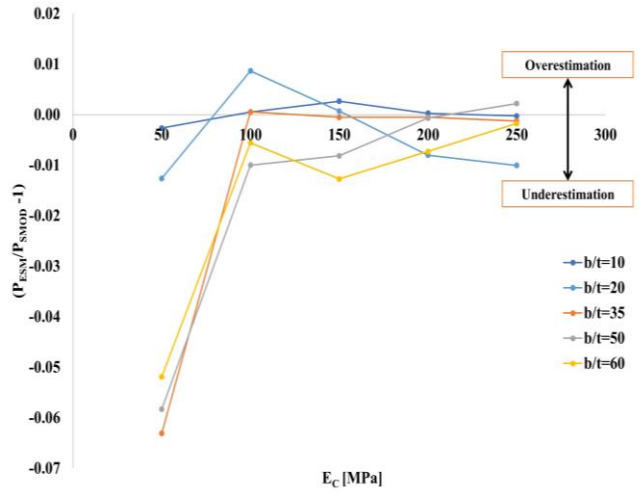

Fig. 9. ESM error using Eq. (3)

5. Application of ESM

5.1. Numerical Model of PAC-Encased C-Profiles

To show the potential of the ESM, it was applied for a set of different compression elements previously reported in [1], [21], [22]. Altogether, 27 specimens were used during the model validation. The ESM model was built in ANSYS to simulate the test series described in Table 3. C90 sections had 90 mm web height, and C140 had 140mm. In all cases, the flange width and the edge stiffener were 41 mm and 13 mm, respectively. The plate thickness ranged from 0.9 to 1.5 mm, with element lengths of either 300 mm or 600 mm. The material grade of the tested CFS was DX51D+Z. Besides, the end configuration was different in tests; see Fig. 11. The cold-formed steel C-section was modelled using 4-node SHELL181 elements with a bilinear elastic-plastic material law with von Mises yield criterion and isotropic hardening, following the modelling guidelines in EC3-1-5 [28]. The elastic modulus (E) of the steel was set to 210 GPa, the Poisson's ratio to 0.3, and the yield strength determined from coupon tests. The PAC block was replaced with COMBIN40 element, with spring stiffness calculated using Eq. (3) for outstanding (stiffeners) and, Eq. (4) (reported in [26]) for internal elements (web and flanges). E_C was set to 50 MPa as an average value [21].

$$K = -203.2 + 5.231A + 1.942E_c - 0.02615A^2 + 0.02615AE_c + 0.001267E_c^2 \quad (4)$$

A mesh sensitivity study was conducted to identify the optimal mesh size, concluding that a maximum element size of 2.5 mm for steel and 5 mm for PAC provided the most accurate performance within the investigated experimental range. The complicated end configuration was eliminated from the model, and load transfer was represented by eccentric support nodes connected to the end of the specimen by rigid regions. In boundary conditions, support nodes were created at the C-section centre at both ends to establish rigid regions. The specimen's bottom end was modelled with hinged support, while roller support in the vertical direction was created for the top end. Additionally, rotation along the vertical Z-axis (Rz) was restricted at both ends to prevent torsional movements. Moreover, all PAC equivalent springs were restrained in the normal direction (see Fig. 10). The spring behaviour was assumed to be linearly elastic, excluding considerations of cracking, crushing, bonding or friction.

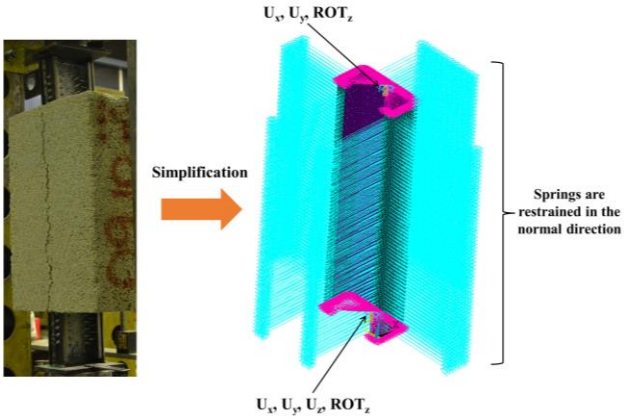

Fig.10. ESM 3D model illustration and boundary conditions

5.2. Equivalent Geometric Imperfection and Initial Eccentricity

The nonlinear analysis incorporated both material nonlinearity and geometric imperfections of the steel (GMNIA). Geometric imperfections were defined as the lowest eigen-shape of the encased model, scaled by an amplitude of b/200 and b/50 for internal and outstanding plates, respectively. An initial load eccentricity of 6 mm was considered in the verification process for the following reasons:

1. In the first test series [21], the load was applied from a hot-rolled frame through four sets of screws attached solely to the web and flanges rather than over the entire section (see Fig. 11A).
2. The required eccentricity can be estimated in two different ways: by summing the bending moments over the C-section centre ($e = \frac{\sum M}{F_{test}}$), assuming equal load distribution through all screws, or by calculating the offset between the center of the load frame and the C-section profile. The calculated eccentricity was found to range from 4 to 7 mm.
3. Regarding the second test series [22], given that both the C and U sections have the same height and due to rounded corners, a gap always exists between the two sections (see Fig. 11B). Hence, a 2 mm thick L-section was used to close this gap and increase the web stiffness. This configuration resulted in an eccentricity in the applied towards the section web.

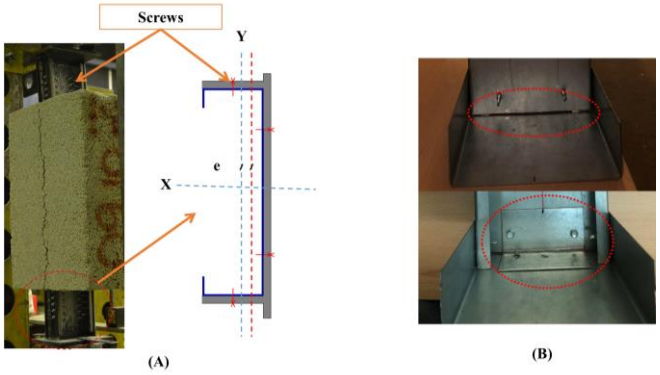

Fig.11. A) First test series [22], B) second test configuration

5.3. Evaluation of Ultimate Strength

A GMNIA was conducted to determine the ultimate strength for two different section heights, specifically C90 and C140, following the analysis steps outlined in Figure 12. Based on FE outcomes, the analysis demonstrated that the ESM closely matched the experimental results, with a root mean square error (RMSE) of 6%, see Table 3. Similar to the experimental test, local failure phenomena governed the ESM model failure. To illustrate the ESM's performance, Figure 13 depicts the ESM failure mode compared to the experimental (note that the load transferring self-drilling screws were eliminated from the model). Consequently, the verification demonstrated the efficiency and applicability of ESM as an effective analysis tool, and hence, using it in modelling continuous elastic bracing is deemed favourable.

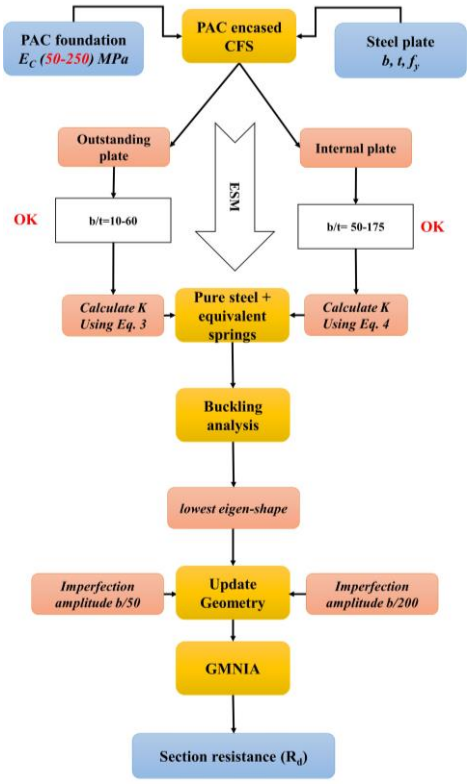

Fig. 12. Flowchart of modelling by ESM

TABLE 3. ESM result compared to the experimental tests

Notation	Measured thickness [mm]	Yield strength [N/mm2]	Test result [kN]	ESM result [kN]	F_{ESM}/F_{Test}-1
C90-10-300-A*1	0.84	372	38.93	38.2	-0.02
C90-10-600-A*1	0.84		37.8	37.7	0.00
C140-10-300*1	0.92	314	40.53	43.47	0.07
C140-10-600*1	0.94		40.08	43.43	0.08
C140-15-600*1	1.52	305	79.56	83.8	0.05
C90-10-300*2	0.84	372	35.73	38.2	0.07
C90-15-300*2	1.41	355	66.52	70.55	0.06
C140-10-600*2	0.88	343	46.18	44.75	-0.03
C140-15-300*2	1.44	282	72.44	76.24	0.05
RMSE					0.06

*1 Experimental test reported in [21]
*2 Experimental test reported in [22]

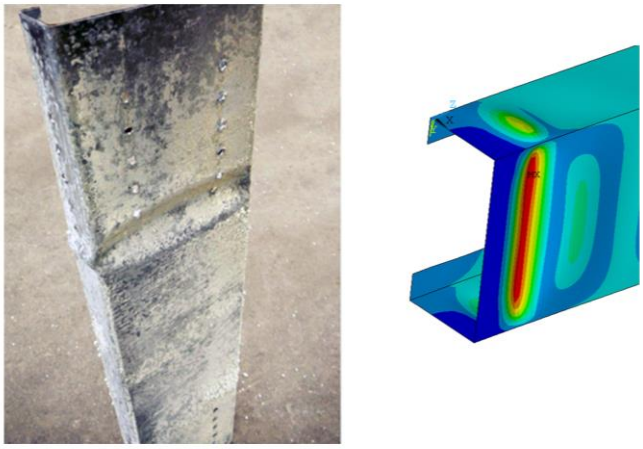

Fig. 13. Failure mode comparison of ESM

6. CONCLUSIONS

In this study the equivalent spring method (ESM) representing the effect of the elastic infill material of encased cold-formed steel sections was investigated. First, the performance of the ESM was compared to 3-D solid model (SMOD) results on a practical parameter range of outstand plate elements regarding the ultimate failure load, load-displacement curve and failure mode. It was shown that the prediction of ESM on the ultimate load, failure mode and load-displacement curve is in good agreement with the SMOD results for a wide range of elastic modulus (50–250 MPa) with maximum difference less than 5 %. A simplification in determining the equivalent spring stiffness was proposed to slightly reduce the complexity of the method. The analysis results showed that this simplification can give acceptable results compared to 3-D model, with a maximum error of 6 %. Next, the application of ESM was shown and discussed using a large set of experiments. The analysis outcomes demonstrated that ESM helps to adequately identify the ultimate load of the encased CFS sections with less computational effort. Hence, this proposed model can be

applied to various cross-section configurations, including C-sections, box-sections, hat shapes, and U-sections within the parameter range of its application.

ACKNOWLEDGEMENTS

The authors gratefully acknowledge the support of the Hungarian Government and the Tempus Public Foundation for funding this research project as part of the Stipendium Hungaricum Scholarship scheme within a doctoral program.

REFERENCES

[1] A. Alabedi, P. Hegyi, Development of a Eurocode-based design method for local and distortional buckling for cold-formed C-sections encased in ultra-lightweight concrete under compression, Thin-Walled Structures 196 (2024) 111504. https://doi.org/10.1016/j.tws.2023.111504.

[2] P. Hegyi, L. Dunai, Experimental study on ultra-lightweight-concrete encased cold-formed steel structures Part I: Stability behaviour of elements subjected to bending, Thin-Walled Structures 101 (2016) 75–84. https://doi.org/10.1016/j.tws.2016.01.004.

[3] H. Wu, S. Chao, T. Zhou, Y. Liu, Cold-formed steel framing walls with infilled lightweight FGD gypsum Part II: Axial compression tests, Thin-Walled Structures 132 (2018) 771–782. https://doi.org/10.1016/j.tws.2018.06.034.

[4] C. Yin, L. Zhou, Q. Zou, Y. Xu, Effect of Filling Phosphogypsum on the Axial Compression Behavior of Cold-Formed Thin-Walled Steel Walls, Buildings 12 (2022) 1325. https://doi.org/10.3390/buildings12091325.

[5] Z. Xu, Z. Chen, B.H. Osman, S. Yang, Seismic performance of high-strength lightweight foamed concrete-filled cold-formed steel shear walls, J Constr Steel Res 143 (2018) 148–161. https://doi.org/10.1016/j.jcsr.2017.12.027.

[6] Z. Xu, Z. Chen, S. Yang, Seismic behavior of cold-formed steel high-strength foamed concrete shear walls with straw boards, Thin-Walled Structures 124 (2018) 350–365. https://doi.org/10.1016/j.tws.2017.12.032.

[7] Z. Xu, Z. Chen, S. Yang, Effect of a new type of high-strength lightweight foamed concrete on seismic performance of cold-formed steel shear walls, Constr Build Mater 181 (2018) 287–300. https://doi.org/10.1016/j.conbuildmat.2018.06.067.

[8] W. Wang, J. Wang, T.Y. Yang, L. Guo, H. Song, Experimental testing and analytical modeling of CFS shear walls filled with LPM, Structures 27 (2020) 917–933. https://doi.org/10.1016/j.istruc.2020.06.016.

[9] W. Wang, J. Wang, P. Zhao, L. Ja, G. Pan, Axial compressive experiments and structural behaviour estimation of CFS composite walls sprayed with LPM, Journal of Building Engineering 30 (2020) 101305. https://doi.org/10.1016/j.jobe.2020.101305.

[10] W. Wang, J. Wang, L. Guo, Mechanical behavior analysis of LEM-infilled cold-formed steel walls, Sustainable Structures 2 (2022). https://doi.org/10.54113/j.sust.2022.000013.

[11] M.A. Othuman Mydin, Y.C. Wang, Structural performance of lightweight steel-foamed concrete–steel composite walling system under compression, Thin-Walled Structures 49 (2011) 66–76. https://doi.org/10.1016/j.tws.2010.08.007.

[12] E.A. Flores-Johnson, Q.M. Li, Structural behaviour of composite sandwich panels with plain and fibre-reinforced foamed concrete cores and corrugated steel faces, Compos Struct 94 (2012) 1555–1563. https://doi.org/10.1016/j.compstruct.2011.12.017.

[13] E. Eltayeb, X. Ma, Y. Zhuge, O. Youssf, J.E. Mills, J. Xiao, A. Singh, Structural performance of composite panels made of profiled steel skins and foam rubberised concrete under axial compressive loads, Eng Struct 211 (2020) 110448. https://doi.org/10.1016/j.engstruct.2020.110448.

[14] E. Eltayeb, X. Ma, Y. Zhuge, J. Xiao, O. Youssf, Composite walls Composed of profiled steel skin and foam rubberized concrete subjected to eccentric compressions, Journal of Building Engineering 46 (2022) 103715. https://doi.org/10.1016/j.jobe.2021.103715.

[15] A. Sheta, X. Ma, Y. Zhuge, M. ElGawady, J.E. Mills, E. Abd-Elaal, Axial compressive behaviour of thin-walled composite columns comprise high-strength cold-formed steel and PE-ECC, Thin-Walled Structures 184 (2023) 110471. https://doi.org/10.1016/j.tws.2022.110471.

[16] F.M.D.S. More, S.S. Subramanian, Experimental Investigation on the Axial Compressive Behaviour of Cold-Formed Steel-Concrete Composite Columns Infilled with Various Types of Fibre-Reinforced Concrete, Buildings 13 (2023) 151. https://doi.org/10.3390/buildings13010151.

[17] S. R., D. M., D.R. S., B. A., S. Avudaiappan, K.D. Tsavdaridis, Behaviour of cold-formed steel-concrete composite columns under axial compression: Experimental and numerical study, Structures 44 (2022) 487–502. https://doi.org/10.1016/j.istruc.2022.07.086.

[18] Y. Li, X. Wu, X. Li, K. Zhang, C. Gao, Compression Performance and Calculation Method of Thin-Walled Prefabricated Steel Tube Lightweight Concrete Columns, Advances in Civil Engineering 2022 (2022) 1–11. https://doi.org/10.1155/2022/2011786.

[19] B. Yao, H. Fang, Z. Qian, Q. Wang, J. Sun, W. Wang, Experimental and Numerical Study on Axial Compression Cold-Formed Steel Composite Wall under Concentrated Loads, Buildings 13 (2023) 1232. https://doi.org/10.3390/buildings13051232.

[20] É. Lublóy, L.G. Balázs, K. Kopecskó, E. Tóth, L. Dunai, P. Hegyi, O. Drávucz, Thermal insulation capacity of concretes by expanded polystyrene aggregate, Improving Performance of Concrete Structures (2014).

[21] P. Hegyi, L. Dunai, Experimental investigations on ultra-lightweight-concrete encased cold-formed steel structures, Thin-Walled Structures 101 (2016) 100–108. https://doi.org/10.1016/j.tws.2016.01.003.

[22] P. Hegyi, L. Dunai, Experimental Investigation of Thin-walled Column-end Joints Encased in Ultra-lightweight Concrete, Periodica Polytechnica Civil Engineering 61 (2017) 951–957. https://doi.org/10.3311/PPci.10041.

[23] P. Hegyi, L. Horváth, L. Dunai, A.A.M. Ghazi, Experimental Investigation of Shear Effects in Ultra-Lightweight Concrete Encased CFS Structural Members, Ce/Papers 5 (2022) 143–150. https://doi.org/https://doi.org/10.1002/cepa.1739.

[24] N. Eid, A.L. Joo, Simplified numerical model development for advanced design of lightweight-concrete encased cold-formed steel compressed elements, Advances in Civil Engineering 2022 (2022).

[25] P. Hegyi, L. Dunai, 07.18: Cold-formed C-sections encased in ultra-lightweight concrete: Development of a Eurocode-based design method, Ce/Papers 1 (2017) 1647–1656. https://doi.org/10.1002/cepa.208.

[26] A. Alabedi, P. Hegyi, Assessing the Equivalent Spring Method for Modelling of Lightweight-concrete Encased Cold-formed Steel Elements in Compression, Periodica Polytechnica Civil Engineering 68 (2023) 305–313. https://doi.org/10.3311/PPci.22803.

[27] Ansys® Academic Research, R2, help system, structural analysis, Guide, ANSYS, (2022).

[28] En 1993-1-5, Eurocode 3, Design of Steel Structures, Part 1–5: Plated Structural Elements, in: CEN, Bruxelles, 2006.

[29] J. Becque, An Analytical Design Approach for Outstand Steel Plates in Compression, Ce/Papers 6 (2023) 1821–1825. https://doi.org/10.1002/cepa.2535.

[30] K.J.R. Rasmussen, G.J. Hancock, Plate slenderness limits for high strength steel sections, J Constr Steel Res 23 (1992) 73–96. https://doi.org/10.1016/0143-974X(92)90037-F.

[31] J. Nie, H. Sugimoto, K. Ono, T. Miyashita, M. Matsumura, S. Okada, An experimental study on the local buckling strength of an SBHS700 stub column with cruciform section: With an overview of the mechanical properties of SBHS700, Steel Construction 12 (2019) 82–90.

[32] P.B. Dinis, D. Camotim, Buckling, post-buckling and strength of cruciform columns, in: USB Key Drive Proceedings of SSRC Annual Stability Conference (Pittsburgh, 9-14/5), 2011.

[33] O.S. Hopperstad, M. Langseth, T. Tryland, Ultimate strength of aluminium alloy outstands in compression: experiments and simplified analysis, Thin-Walled Structures 34 (1999) 279–294. https://doi.org/10.1016/S0263-8231(99)00013-0.